Bichromatic electromagnetically induced transparency in hot atomic vapors

Hui Yan,[1,*] Kai-Yu Liao,[1] Jian-Feng Li,[1] Yan-Xiong Du,[1] Zhi-Ming Zhang,[2] and Shi-Liang Zhu[1,†]

[1]*Laboratory of Quantum Information Technology, School of Physics and Telecommunication Engineering, South China Normal University, Guangzhou 510006, China*

[2]*Laboratory of Quantum Information Technology, School of Information and Photoelectronic Science and Engineering, South China Normal University, Guangzhou 510006, China*

(Received 29 November 2012; published 1 May 2013)

In a three-level Λ atomic system coupled by a symmetrical bichromatic laser field, a weak probe laser field shows multiple absorption peaks in the case of cold atoms. As for hot atomic vapors, we experimentally observe double symmetrical electromagnetically induced transparency windows instead of multiple absorption peaks. This abnormal spectrum is due to the Doppler averaging. The electromagnetically induced transparency windows observed here are useful for obtaining slow photons at different frequencies.

DOI: 10.1103/PhysRevA.87.055401 PACS number(s): 32.80.Qk, 42.50.Gy, 42.50.Dv

Electromagnetically induced transparency (EIT) has many applications in various fields of physics [1,2]. One of the most promising applications is that EIT can be used in entangling photons through cross-phase modulation [3–13]. In order to achieve a significant cross-phase modulation between photons, long atom-photon interaction time is one of the main requirements. Therefore, utilizing double symmetrical EIT windows to match the slow group velocity of two photons is the benchmark for large cross-phase modulation. One possible way to achieve double symmetrical EIT windows is utilizing bichromatic EIT [14–20]. The first experiment of bichromatic EIT was done with cold atoms by Wang *et al*. [18]. In their experiment, multiple absorption peaks were observed. However, for bichromatic EIT with cold atoms, the slope of the normal dispersion is related to the frequency of the coupling laser and large slowing can be obtained just at a fixed frequency, which will limit its application. On the other hand, many theoretical proposals for cross-phase modulations and related applications are based on hot atomic vapors [21–30]. Narrow EIT window, the jumping-off point for slowing light, has already been demonstrated with hot atomic vapors because of the Doppler averaging [31,32]. However, the bichromatic or multiple EIT with hot atomic vapors is a relatively unexplored topic.

In this Brief Report, we report an experimental study of bichromatic EIT in a hot atomic vapor. Each atom in the vapor has a three-level Λ configuration coupled by a bichromatic laser field. Rather than the absorption spectrum with multiple peaks observed in cold atoms, double symmetrical narrow EIT windows are observed in our experiments. This bichromatic EIT spectrum can be understood by considering the Doppler averaging. We numerically calculate the probe laser spectrums of the hot atomic vapors through averaging over one-dimensional Maxwell-Boltzmann velocity distribution and find that the theoretical results fit pretty well with the experimental results. The system with double symmetrical narrow EIT windows observed here provides a good medium for obtaining slow photons at different frequencies and can be used to achieve a large cross-phase modulation.

*yanhui@scnu.edu.cn
†slzhu@scnu.edu.cn

We consider an atomic gas with each atom having a Λ-type level configuration as shown in Figs. 1(a) and 1(d). The excited state $|3\rangle$ is coupled with the ground state $|1\rangle$ through a symmetrical bichromatic laser field with the corresponding Rabi frequencies Ω_{c1} and Ω_{c2}, and it is coupled to another ground state $|2\rangle$ through a probe laser with Rabi frequency Ω_p. We denote $\hbar\omega_j$ as the energy of the state $|j\rangle$ and $\omega_{ij} = \omega_i - \omega_j$ $(i > j)$ is the transition frequency between energy levels $|i\rangle$ and $|j\rangle$. Without loss of generality, we assume $\omega_2 = 0$. Under the rotating-wave and dipole approximations, the entire Hamiltonian can be described in a weak probe field condition as

$$H = -\hbar\Delta_p|3\rangle\langle 3| - \hbar(\Delta_p - \Delta_0)|1\rangle\langle 1| - \frac{\hbar}{2}[(\Omega_1 e^{-i\delta_1 t} + \Omega_2 e^{-i\delta_2 t})|3\rangle\langle 2| + \Omega_p|3\rangle\langle 1| + \text{H.c.}], \tag{1}$$

where $\Delta_0 = \omega_{13} - (\delta_1 + \delta_2)/2$ with δ_1, δ_2, and Δ_p being the detunings of the coupling and probe fields, respectively. The density-matrix elements ρ_{jk} can be calculated from the master equation

$$\dot{\rho} = -\frac{i}{\hbar}[H,\rho] + \dot{\rho}_d, \tag{2}$$

where $\dot{\rho}_d$ stand for all of the damping terms. Substituting Eq. (1) into Eq. (2), we have

$$\dot{\rho}_{11} = \frac{i}{2}\Omega_p^*\rho_{31} - \frac{i}{2}\Omega_p\rho_{13} + \gamma_1(1 - \rho_{11} - \rho_{22}), \tag{3}$$

$$\dot{\rho}_{22} = \frac{i}{2}(\Omega_1^* e^{-i\delta t} + \Omega_2^* e^{i\delta t})\rho_{32} - \frac{i}{2}(\Omega_1 e^{i\delta t} + \Omega_2 e^{-i\delta t})\rho_{23} + \gamma_2(1 - \rho_{11} - \rho_{22}), \tag{4}$$

$$\dot{\rho}_{31} = -\frac{1}{2}(\gamma_1 + \gamma_2 - i\Delta_p)\rho_{31} + \frac{i}{2}(\Omega_1 e^{i\delta t} + \Omega_2 e^{-i\delta t})\rho_{21} + \frac{i}{2}\Omega_p(2\rho_{11} + \rho_{22} - 1), \tag{5}$$

$$\dot{\rho}_{32} = -\frac{1}{2}(\gamma_1 + \gamma_2 - i\Delta_0)\rho_{32} + \frac{i}{2}\Omega_p\rho_{12} + \frac{i}{2}(\Omega_1 e^{i\delta t} + \Omega_2 e^{-i\delta t})(2\rho_{22} + \rho_{11} - 1), \tag{6}$$

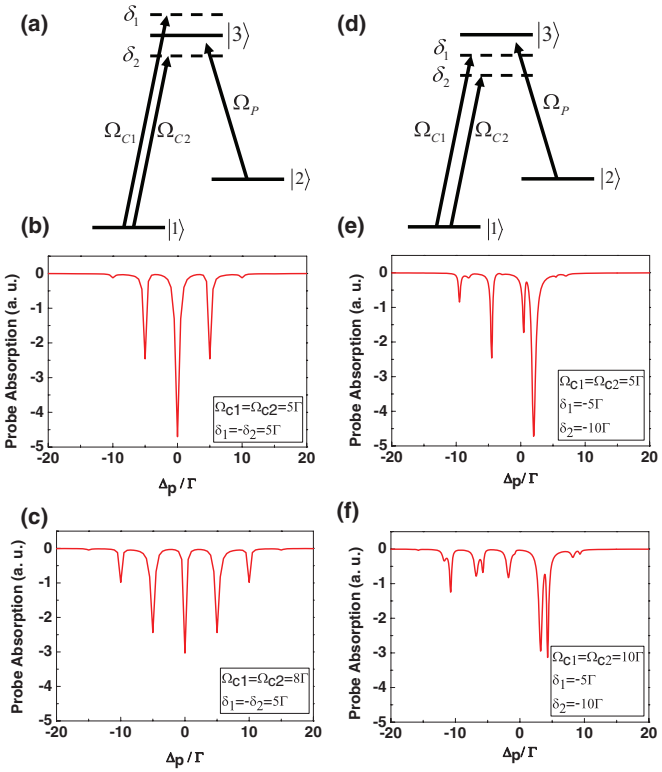

FIG. 1. (Color online) Schematic representation of the light-atom interaction for bichromatic EIT and the probe absorption spectrum of the cold atoms obtained through the numerical simulations. (a)–(c) Symmetrical probe absorptions for $\delta_1 = -\delta_2 = 5\Gamma = 30$ MHz; (d)–(f) unsymmetrical probe absorptions for $\delta_1 = -5\Gamma$, $\delta_2 = -10\Gamma$; (b), (e) $\Omega_{c1} = \Omega_{c2} = 5\Gamma$; (c), (f) $\Omega_{c1} = \Omega_{c2} = 10\Gamma$.

$$\dot{\rho}_{21} = -i(\Delta_0 - \Delta_p)\rho_{21} - \frac{i}{2}\Omega_p\rho_{23} + \frac{i}{2}(\Omega_1^* e^{-i\delta t} + \Omega_2^* e^{i\delta t})\rho_{31}, \tag{7}$$

together with the relationships $\rho_{13} = \rho_{31}^*$, $\rho_{23} = \rho_{32}^*$, and $\rho_{12} = \rho_{21}^*$. Here, $\delta = (\delta_1 - \delta_2)/2$ and γ_j $(j = 1,2)$ describe the decay from $|3\rangle$ to $|j\rangle$.

To obtain the numerical solutions of the above time-dependent master equations, we expand ρ_{jk} in terms of Fourier components as

$$\rho_{jk}(t) = \sum_{l=-\infty}^{l=\infty} \rho_{jk}^{(l)}(t) e^{il\delta t} \quad (j,k = 1,2,3). \tag{8}$$

Here, $\rho_{jk}^{(l)}(t)$ represent the slowly varying amplitudes, which may be used to determine the absorption part χ' and dispersion part χ'' of the optical medium, i.e.,

$$\chi' = \frac{n_a |d_{23}|^2}{\varepsilon_0 \hbar} \mathrm{Re}\left(\frac{\rho_{32}^{(0)}}{\Omega_p}\right), \tag{9}$$

$$\chi'' = \frac{n_a |d_{23}|^2}{\varepsilon_0 \hbar} \mathrm{Im}\left(\frac{\rho_{32}^{(0)}}{\Omega_p}\right). \tag{10}$$

The n_a in Eqs. (9) and (10) is the density of the atoms, and d_{23} is the dipole moment between $|2\rangle$ and $|3\rangle$. Equations (8)–(10) can be solved by a matrix inversion method [33]. The probe absorptions for typical parameters are plotted in Figs. 1(b), 1(c), 1(e), and 1(f). As shown in Figs. 1(a)–1(c), when the bichromatic coupling laser fields are symmetrical ($\Omega_{c1} = \Omega_{c2} = 5\Gamma$, $\delta_1 = -\delta_2 = 5\Gamma$ with $\Gamma \sim 6$ MHz; rubidium is under consideration), the probe absorption spectrum displays some peaks at $0, \pm\delta, \pm 2\delta, \ldots$. By increasing the Rabi frequencies of the coupling fields, more peaks will appear. If the bichromatic fields are unsymmetrical, e.g., $\delta_1 = -5\Gamma, \delta_2 = -10\Gamma$, the positions of the peaks in the probe absorption spectrum shift, as shown in Figs. 1(d)–1(f). Thus the maximum absorptions are no longer located at the two-photon resonant points.

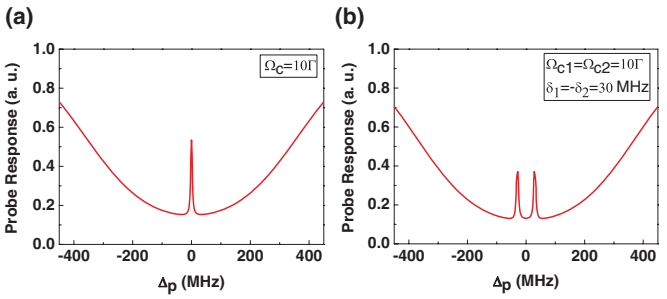

FIG. 2. (Color online) The calculated probe absorptions of the hot atomic vapors for monochromatic EIT and bichromatic EIT. (a) Monochromatic EIT, $\Omega_c = 10\Gamma$; (b) bichromatic EIT, $\Omega_{c1} = \Omega_{c2} = 10\Gamma$, $\delta_1 = -\delta_2 = 5\Gamma = 30$ MHz.

Until now, all of our analyses are valid for stationary atoms (or valid for cold atoms). For the hot atomic vapors, all atoms move very fast in the cell. If an atom has a velocity v along the laser propagation direction, the detuning will change by kv ($k = \frac{2\pi}{\lambda}$, with λ being the wavelength of the laser). Therefore, in order to obtain the entire probe absorption spectrum for hot atoms, the detuning in the density-matrix elements should also include the Doppler frequency shift, which varies with the velocity of the atoms. Thus, ρ_{jk} should be averaged over the one-dimensional Maxwell-Boltzmann velocity distribution given by [34]

$$\rho_{jk} = \int \rho_{jk}(\Delta + kv) \frac{1}{u\sqrt{\pi}} e^{-v^2/u^2} dv, \tag{11}$$

where Δ stands for all the detuning terms, and $u/\sqrt{2}$ is the root-mean-square atomic velocity (depending on the temperature of the cell).

Based on Eq. (11), the probe absorption spectrum can be calculated out for hot atomic vapors. For comparison, both monochromatic and bichromatic EIT spectrums with Doppler broaden and are plotted in Fig. 2. When $\Omega_c = 10\Gamma$, $T = 70\,^\circ$C (with T being the temperature of the atomic cell), the linewidth of the EIT window is about 6 MHz, as shown in Fig. 2(a). In the same condition, considering a bichromatic coupling field with $\Omega_{c1} = \Omega_{c2} = 10\Gamma$, $\delta_1 = -\delta_2 = 5\Gamma = 30$ MHz, two symmetric EIT windows appear at δ_1 and δ_2, as shown in Fig. 2(b). This abnormal bichromatic EIT spectrum is surprising; however, it can be understood by considering the different bichromatic EIT line shape for the atoms with different velocities. If the atoms move with the velocity v, the coupling bichromatic fields will be unsymmetrical due to the Doppler frequency shift, and the position of the probe absorption peaks will shift

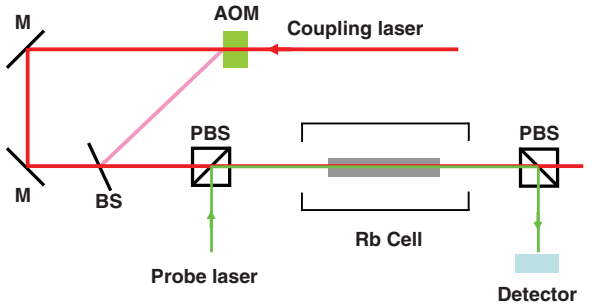

FIG. 3. (Color online) The experimental configuration. AOM: acousto-optic modulator; M: mirror; BS: beam splitter; PBS: polarization beam splitter; Rb Cell: rubidium cell with magnetic shield and temperature controller.

from the two-photon resonant points. For example, assuming that $v = 6$ m/s, the detuning of the bichromatic fields will change to $\delta_1 = -5\Gamma, \delta_2 = -10\Gamma$, and the absorption peaks will shift from $\pm 5\Gamma$, as shown in Figs. 1(e) and 1(f). Since all atoms are moving, after the Doppler averaging, only two EIT windows appear and the other frequencies have big absorption.

We now turn to the experimental demonstration of these results. The experimental setup is shown in Fig. 3. The coupling and probe laser beams are derived from two independent diode lasers (DL100, 795 nm). The coupling laser is frequency stabilized through a saturated-absorption spectrum technique. The diameters of the two beams are about 2 mm. An acousto-optic modulator (AOM) is adapted to generate the bichromatic field with a tunable frequency separation (between 40 and 80 MHz). These beams are combined by a beam splitter (BS) and a polarization beam splitter (PBS). They copropagate through a 10-cm-length cell with natural rubidium. The cell has a magnetic shield around it so that the residual magnetic field $B < 1$ mG. A temperature controller is also equipped with the cell so that the cell can be heated to 70 °C. After the cell, another PBS (extinction ratio 10^{-5}) is used to split the probe beam from the coupling beams.

The three energy levels of the Λ system are selected as ^{85}Rb, $5S_{1/2}, F = 3 \rightarrow |1\rangle$, $5S_{1/2}, F = 2 \rightarrow |2\rangle$, and $5P_{1/2}, F = 3 \rightarrow |3\rangle$. We first use the bichromatic laser fields to couple $|1\rangle \leftrightarrow |3\rangle$ with $\Omega_{c1} = \Omega_{c2} = 9.3\Gamma$ (limited by the maximum power of the laser), and $\delta_1 = -\delta_2 = 30$ MHz, while the probe laser scans about 600 MHz around $|2\rangle \rightarrow |3\rangle$ with $\Omega_p \sim \Gamma$. The experimental results of the probe absorptions are shown in Fig. 4. As expected from the theoretical calculations, we observe two symmetrical EIT windows. The linewidths of both windows are narrower than the natural linewidth Γ. For comparison, the probe absorptions for only one of the coupling lasers are also collected, and the results are also plotted in Fig. 4. Both the monochromatic and abnormal bichromatic EIT spectrums agree pretty well with the theoretical results based on Eq. (11), as shown in Fig. 2. The decreasing of the absorption at the EIT window bottom is another evidence for the Doppler averaging. In addition, the absorption around -360 MHz, which is precisely the hyperfine interval between the $5P_{1/2}, F^{'} = 2$ and $F^{'} = 3$, is due to additional velocity-dependent optical pumping by the control laser.

As shown in Fig. 5(a), these narrow symmetric double EIT windows are ideal for slowing photons with a fixed frequency

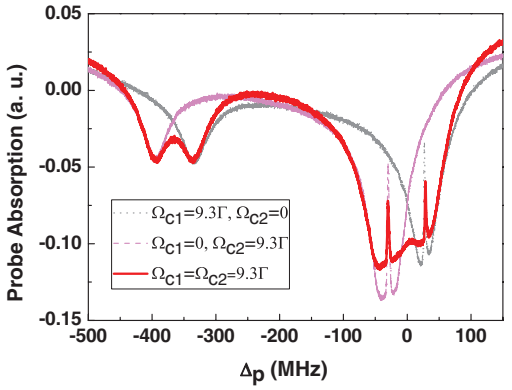

FIG. 4. (Color online) Probe absorption as a function of the detuning of the probe laser for the $5S_{1/2}, F = 2 \rightarrow 5P_{1/2}$ transition of ^{85}Rb D_1 line. Solid red line: bichromatic EIT, $\Omega_{c1} = \Omega_{c2} = 9.3\Gamma$, $\delta_1 = -\delta_2 = 30$ MHz. Dotted black line: monochromatic EIT, $\Omega_{c1} = 9.3\Gamma$, $\Omega_{c2} = 0$, and $\delta_1 = 30$ MHz. Dashed pink line: monochromatic EIT, $\Omega_{c1} = 0$ $\Omega_{c2} = 9.3\Gamma$, $\delta_2 = -30$ MHz.

difference. In order to show the robust manipulations of these EIT windows, the parameters of the bichromatic laser fields are altered in the experiments. First, as shown in Fig. 5(b), both the heights and linewidths of the two EIT windows decrease with the Rabi frequencies of the coupling lasers simultaneously,

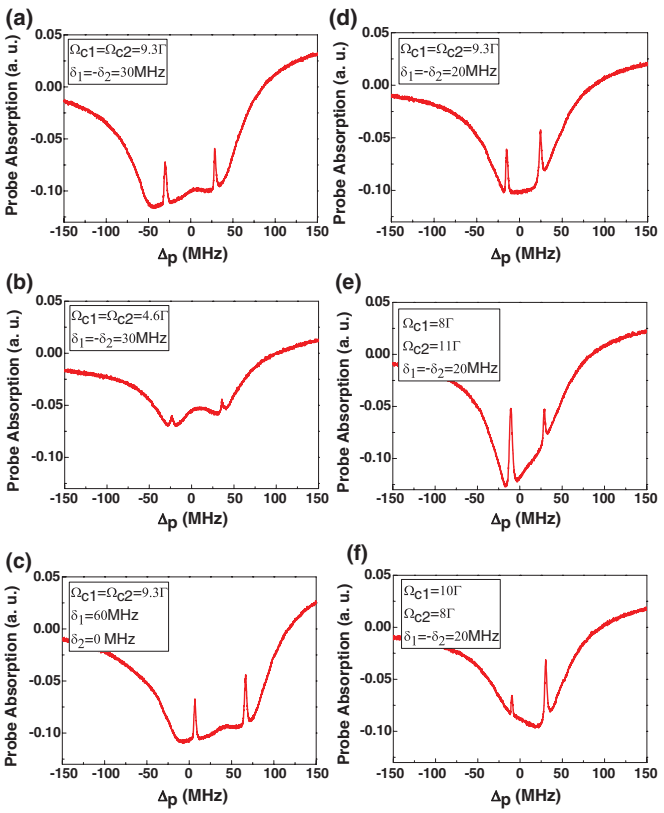

FIG. 5. (Color online) Probe absorption as a function of the detuning of the probe laser. (a) $\Omega_{c1} = \Omega_{c2} = 9.3\Gamma$, $\delta_1 = -\delta_2 = 30$ MHz; (b) $\Omega_{c1} = \Omega_{c2} = 4.6\Gamma$, $\delta_1 = -\delta_2 = 30$ MHz; (c) $\Omega_{c1} = \Omega_{c2} = 9.3\Gamma$, $\delta_1 = 60$ MHz, $\delta_2 = 0$ MHz; (d) $\Omega_{c1} = \Omega_{c2} = 9.3\Gamma$, $\delta_1 = -\delta_2 = 20$ MHz; (e) $\Omega_{c1} = 8\Gamma$,$\Omega_{c2} = 11\Gamma$, $\delta_1 = -\delta_2 = 20$ MHz; (f) $\Omega_{c1} = 10\Gamma$,$\Omega_{c2} = 8\Gamma$, $\delta_1 = -\delta_2 = 20$ MHz.

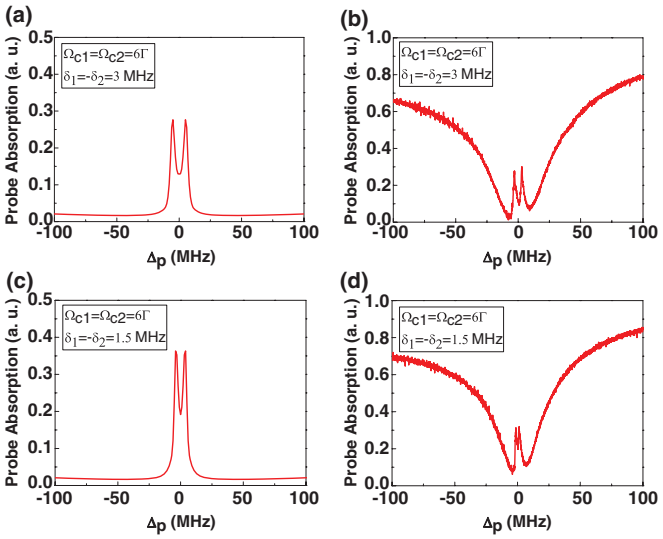

FIG. 6. (Color online) Probe absorption as a function of the detuning of the probe laser. (a), (b) $\Omega_{c1} = \Omega_{c2} = 6\Gamma$, $\delta_1 = -\delta_2 = 3$ MHz; (c), (d) $\Omega_{c1} = \Omega_{c2} = 6\Gamma$, $\delta_1 = -\delta_2 = 1.5$ MHz; (a), (c) theoretical results; (b), (d) experimental results.

which means that the slope of the normal dispersion is related to the Rabi frequencies of the coupling lasers; this phenomena is similar to that of the monochromatic EIT. Second, we alter the center frequency and the detuning of the bichromatic laser field. As shown in Fig. 5(c), with $\delta_1 = 60$ MHz and $\delta_2 = 0$ MHz, the line shape of the double EIT windows is still unchanging. As shown in Fig. 5(d), with $\delta_1 = -\delta_2 = 20$ MHz, almost the same slope of the dispersion can be obtained. In addition, by coupling the levels with unbalanced laser fields, i.e., $\Omega_{c1} \neq \Omega_{c2}$, the double unbalanced EIT windows appear in the spectrum, as shown in Figs. 5(e) and 5(f). All of these show that the double EIT windows can be controlled separately or simultaneously on demand. Thus, by applying these double EIT windows to slow the photons, the velocity of each photon can be controlled separately [35–37].

Furthermore, in order to decrease the detuning of bichromatic laser fields, another AOM is added in one of the coupling beams. As shown in Fig. 6, by decreasing the detuning below the natural linewidth (with detunings 3 and 1.5 MHz), the double EIT windows move toward each other and finally may combine together. The theoretical results are shown in Figs. 6(a) and 6(c), and the windows of EIT fit pretty well with the experimental results [Figs. 6(b) and 6(d)] with the same parameters. The differences of the big absorption backgrounds are due to the optical pumping of the control laser for zero velocity atoms [32]. Those results show that the double EIT windows can be controllable independently until they combine together at a very small detuning.

In conclusion, through coupling a three-level Λ atomic system by the symmetrical bichromatic laser fields, we have observed that a weak probe laser field shows double symmetrical narrow EIT windows in hot atomic vapors. The theoretical results by averaging over one-dimensional Maxwell-Boltzmann velocity distribution are found to fit pretty well with the experimental results. Compared with the double EIT windows from tripod or *M*-type energy levels [10], the independent manipulation of either one of the EIT windows will make the match of the slow group velocity more easily. Thus, this abnormal bichromatic EIT is an ideal medium for slowing photons at different frequencies and can be used to obtain larger cross-phase modulations. In particular, it is very suitable for the storage of the entangled photons generated through bichromatic four-wave mixing [38–40]. Therefore, the bichromatic EIT observed in the present experiment may find applications in quantum information processing.

We thank X. M. Hu and G. Q. Yang for helpful discussions. This work was supported by the NSF of China (Grants No. 11104085 and No. 11125417), the Major Research Plan of the National Natural Science Foundation of China (Grant No. 91121023), the SKPBR of China (Grant No. 2011CB922104), and PCSIRT. K.L. and Y.D. were also supported by the SRFGS of SCNU.

[1] M. Fleischhauer, A. Imamoglu, and J. P. Marangos, Rev. Mod. Phys. **77**, 633 (2005).
[2] Y. W. Lin, W. T. Liao, T. Peters, H. C. Chou, J. S. Wang, H. W. Cho, P. C. Kuan, and I. A. Yu, Phys. Rev. Lett. **102**, 213601 (2009).
[3] M. D. Lukin and A. Imamoğlu, Phys. Rev. Lett. **84**, 1419 (2000).
[4] D. Petrosyan and G. Kurizki, Phys. Rev. A **65**, 033833 (2002).
[5] M. D. Lukin and A. Imamoğlu, Nature (London) **413**, 273 (2001).
[6] C. Hang, Y. Li, L. Ma, and G. X. Huang, Phys. Rev. A **74**, 012319 (2006).
[7] A. Joshi and M. Xiao, Phys. Rev. A **72**, 062319 (2005).
[8] Y. Guo, S.-S. Li, and L.-M. Kuang, J. Phys. B: At. Mol. Opt. Phys. **44**, 065501 (2011).
[9] B.-W. Shiau, M.-C. Wu, C.-C. Lin, and Y.-C. Chen, Phys. Rev. Lett. **106**, 193006 (2011).
[10] S. J. Li, X. D. Yang, X. M. Cao, C. H. Zhang, C. D. Xie, and H. Wang, Phys. Rev. Lett. **101**, 073602 (2008).
[11] Z.-B. Wang, K.-P. Marzlin, and B. C. Sanders, Phys. Rev. Lett. **97**, 063901 (2006).
[12] H. L. Ma, C. G. Ye, D. Wei, and J. Zhang, Phys. Rev. Lett. **95**, 233601 (2005).
[13] H. Kang and Y. F. Zhu, Phys. Rev. Lett. **91**, 093601 (2003).
[14] Y. F. Zhu, Q. L. Wu, A. Lezama, D. J. Gauthier, and T. W. Mossberg, Phys. Rev. A **41**, 6574 (1990).
[15] H. Freedhoff and Z. Chen, Phys. Rev. A **41**, 6013 (1990).
[16] G. S. Agarwal, Y. Zhu, D. J. Gauthier, and T. W. Mossberg, J. Opt. Soc. Am. B **8**, 1163 (1991).
[17] Z. Ficek and H. S. Freedhoff, Phys. Rev. A **48**, 3092 (1993).
[18] J. Wang, Y. F. Zhu, K. J. Jiang, and M. S. Zhan, Phys. Rev. A **68**, 063810 (2003).
[19] J. P. Zhang, J. Xu, G. Hernandez, X. M. Hu, and Y. Zhu, Phys. Rev. A **75**, 043810 (2007).
[20] H. Wanare, Phys. Rev. Lett. **96**, 183601 (2006).
[21] Y. Wu and L. Deng, Phys. Rev. Lett. **93**, 143904 (2004).

[22] M. Fleischhauer, A. Imamoglu, and J. P. Marangos, Rev. Mod. Phys. **77**, 633 (2005).
[23] K. Hammerer, A. S. Sorensen, and E. S. Polzik, Rev. Mod. Phys. **82**, 1041 (2010).
[24] L. Deng and M. G. Payne, Phys. Rev. Lett. **98**, 253902 (2007).
[25] C. Hang and G. X. Huang, Phys. Rev. A **82**, 053818 (2010).
[26] B. P. Hou, L. F. Wei, G. L. Long, and S. J. Wang, Phys. Rev. A **79**, 033813 (2009).
[27] X.-M. Hu, G.-L. Cheng, J.-H. Zou, X. Li, and D. Du, Phys. Rev. A **72**, 023803 (2005).
[28] W.-X. Yang, A. X. Chen, L.-G. Si, K. J. Jiang, X. X. Yang, and R.-K. Lee, Phys. Rev. A **81**, 023814 (2010).
[29] M. Arikawa, K. Honda, D. Akamatsu, S. Nagatsuka, K. Akiba, A. Furusawa, and M. Kozuma, Phys. Rev. A **81**, 021605 (2010).
[30] X.-M. Hu, J.-H. Zou, X. Li, D. Du, and G.-L. Cheng, J. Phys. B: At. Mol. Opt. Phys. **38**, 683 (2005).
[31] U. D. Rapol, A. Wasan, and V. Natarajan, Phys. Rev. A **67**, 053802 (2003).
[32] S. M. Iftiquar, G. R. Karve, and V. Natarajan, Phys. Rev. A **77**, 063807 (2008).
[33] Z. Ficek and H. S. Freedhoff, Phys. Rev. A **48**, 3092 (1993).
[34] Y. Q. Li and M. Xiao, Phys. Rev. A **51**, 2703(R) (1995).
[35] L. V. Hau, S. E. Harris, Z. Dutton, and C. H. Behroozi, Nature (London) **397**, 594 (1999).
[36] N. B. Phillips, A. V. Gorshkov, and I. Novikova, Phys. Rev. A **78**, 023801 (2008).
[37] S. Y. Zhou, S. C. Zhang, C. Liu, J. F. Chen, J. M. Wen, M. M. T. Loy, G. K. L. Wong, and S. W. Du, Opt. Express **20**, 24124 (2012).
[38] G. Q. Yang, P. Xu, J. Wang, Y. F. Zhu, and M. S. Zhan, Phys. Rev. A **82**, 045804 (2010).
[39] Y. Liu, J. S. Wu, D. S. Ding, B. S. Shi, and G. C. Guo, New J. Phys. **14**, 073047 (2012).
[40] H. Yan, S. C. Zhang, J. F. Chen, M. M. T. Loy, G. K. L. Wong, and S. W. Du, Phys. Rev. Lett. **106**, 033601 (2011).